$FePO_4.2H_2O$ recovery from acidic phosphate-rich waste streams

Bahgat, Nouran T.; Siddiqui, Aamash; Wilfert, Philipp; Korving, Leon; van Loosdrecht, Mark C.M.

DOI
10.1016/j.watres.2024.121905

Publication date
2024

Document Version
Final published version

Published in
Water Research

Water Research 260 (2024) 121905

Contents lists available at ScienceDirect

Water Research

journal homepage: www.elsevier.com/locate/watres

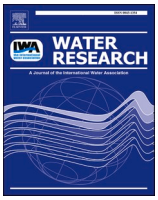

$FePO_4.2H_2O$ recovery from acidic phosphate-rich waste streams

Nouran T. Bahgat [a,b,*], Aamash Siddiqui [a], Philipp Wilfert [b], Leon Korving [a], Mark C.M. van Loosdrecht [b,c]

[a] Wetsus, European Centre Of Excellence for Sustainable Water Technology, Oostergoweg 7, 8911 MA, Leeuwarden, The Netherlands
[b] Department Biotechnology, Delft University of Technology, Van der Maasweg 9, 2629 HZ Delft, The Netherlands
[c] Center for Microbial Communities, Department of Chemistry and Bioscience, Aalborg University, Aalborg, Denmark

ARTICLE INFO

Keywords:
Strengite-like structures
Settleability
Fe (II) oxidation
H_2O_2
SQUID
Raman

ABSTRACT

Phosphorous not only needs to be removed to prevent eutrophication of wastewater effluent receiving surface water bodies, but it also has to be recovered as a scarce finite reserve. Phosphorus chemical precipitation as $NH_4MgPO_4{\cdot}6H_2O$, $Ca_3(PO_4)_2$, or $Fe_3(PO_4)_2\ {\cdot}8H_2O$ is the most common method of phosphorus recovery from phosphorus-rich streams. These minerals ideally form under neutral to alkaline pH conditions, making acidic streams problematic for their formation due to the need for pH adjustments. This study proposes $FePO_4\ .2H_2O$ (strengite-like compounds) recovery from acidic streams due to its simplicity and high efficiency, while also avoiding the need for pH-adjusting chemicals. The effect of initial pH, temperature, Fe (III) dosing rates, and Fe (II) dosage under different oxidation conditions (pO_2 = 0.2, 1, 1.5 bar, different H_2O_2 dosing rates) on phosphorus recovery percentage and product settleability were evaluated in this study. The precipitates formed were analyzed using optical microscopy, SEM, XRD, SQUID, Raman, and ICP. Experiments showed that Fe (III) dosing achieved phosphorus recovery of over 95 % at an initial pH of 3 or higher, and the product exhibited poor settleability in all initial pH (1.5-5), and temperature (20–80 °C) tests. On the other hand, Fe (II) dosage instead of Fe (III) resulted in good product settleability but varying phosphorus recovery percentages depending on the oxidation conditions. The novelty of the study lies in revealing that the Fe (II) oxidation rate serves as a crucial process-design parameter, significantly enhancing product settleability without the requirement of carrier materials or crystallizers. The study proposes a novel strategy with controlled Fe^{2+}-H_2O_2 dosing, identifying an Fe (II) oxidation rate of 4.7×10^{-4} mol/l/min as the optimal rate for achieving over 95 % total phosphorus recovery, along with excellent settleability with a volumetric index equal to only 8 ml/gP.

1. Introduction

Phosphorus is an essential element for life, responsible for various functions in all forms of life, often serving as a limiting nutrient for crops and a crucial component of fertilizers. The primary source of phosphorus is mining phosphate rock, with mined phosphorus primarily utilized for agricultural fertilizers (80 %), along with applications in animal feed additives (5 %), detergents (12 %), metal treatments, and other industrial processes (3 %) (Smit et al., 2009). Despite rising demand, the sustainability of phosphorus use remains uncertain due to diminishing phosphate rock reservoirs and quality concerns arising from cadmium content (Kratz et al., 2016; Ridder, 2012). Moreover, the majority of phosphate reservoirs are concentrated in a few countries, with over 85 % located in Morocco, China, the US, Jordan, and South Africa (Ashley et al., 2011). Regional imbalances in phosphorus distribution can lead to phosphate accumulation or excessive phosphorus discharge into ecosystems, contributing to pollution (van Dijk et al., 2016). Recognizing the critical importance of phosphorus, the European Commission listed phosphorus rock as a critical raw material in 2017 due to its significance for economic development and the risks associated with its supply (Eynard et al., 2020). Consequently, the current EU policy emphasizes phosphorus recovery and improved resource management, aiming to increase the utilization of waste streams for reuse while minimizing losses (ESPP webinar, 2020). This underscores the necessity of cyclic use and phosphorus recovery from secondary sources (Childers et al., 2011).

Phosphorus recovery from wastewater can occur from liquid side streams, sludge, or ash, all of which have high phosphate concentrations. Phosphorus chemical precipitation is the most well-established method for phosphorus recovery from phosphorus-rich streams, utilizing metal salts such as magnesium, calcium, or iron. Mg-struvite

* Corresponding author.
E-mail address: t.m.s.m.bahgat@tudelft.nl (N.T. Bahgat).

https://doi.org/10.1016/j.watres.2024.121905
Received 23 February 2024; Received in revised form 10 May 2024; Accepted 6 June 2024
Available online 9 June 2024

recovery is the most widely implemented technology among commercialized phosphorus recovery techniques due to its simplicity, with struvite crystals forming at pH ≈ 9 (Desmidt et al., 2015; Doyle and Parsons, 2002; Thant Zin and Kim, 2019). Calcium phosphate recovery occurs when calcium is added in the form of Ca $(OH)_2$, and then calcium precipitates with phosphates at pH ≥ 9 (Cichy et al., 2019). To enhance the settleability of struvite and calcium phosphate crystals, crystallizers such as AirPrex®, NuReSys®, Pearl®, Crystalactor®, and PHOSPAQ™ are used (Metcalf and Eddy, 2014). Vivianite (Fe_3 $(PO_4)_2 \cdot 8H_2O$) is also recovered at a pH range of 6-8 when the Fe:P ratio = 1.5. Initially observed in surplus anaerobically digested sludge (Frossard et al., 1997; Wilfert et al., 2016), technology has been developed to crystallize and recover vivianite from liquid streams (Priambodo et al., 2017a). All these techniques for phosphorus recovery require neutral or alkaline pH conditions, as these minerals are soluble under low-pH conditions (Luyckx et al., 2021). This makes phosphorus recovery from low-pH phosphorus-rich streams challenging due to the need for intensive chemical dosing to adjust the pH. It's intriguing that low pH recovery technologies aren't more prevalent, given the substantial impact these streams have on overall phosphorus loads and their widespread presence. The niche of these streams can be separated into:

1) Acidic industrial waste streams: an economically interesting niche for removal and recovery, relatively easy to implement, such as wastewater from cheese production (Carvalho et al., 2013; Danalewich et al., 1998; Lei et al., 2022; Slavov, 2017), wastewater from semiconductors or LCD manufacturing (Martin et al., 2020; Priambodo et al., 2017), wastewater from phosphoric acid production (Monat et al., 2022; Nawghare et al., 2001), wastewater from some pulp and paper industries (Leo et al., 2011; J. C. Zhang et al., 2019), and streams from leaching processes of steelmaking slag (Iwama et al., 2020).
2) Acidic waste streams related to municipal WWTPs: these streams have far bigger phosphorus loads compared to loads from industries (Eicher, 2018; Meyer et al., 2018) as leaching/acidification processes for metal/nutrient recovery of sludge or ash from incinerators. A new niche is wastewater from EPS (Kaumera) extraction processes from aerobic granular sludge (Bahgat et al., 2023). Although the EPS extraction process is quite new, this niche might have high recovery potential as more aerobic granular sludge (Nereda) wastewater plants are established worldwide, and EPS is proving successful as a product. Other potential streams could be identified through further engagement with various industries.

The only available technology to recover phosphorus from these streams is raising the pH to neutral or alkaline conditions (Cichy et al., 2019; Monat et al., 2022), followed by precipitation. Membranes have also been reported as a potential method to concentrate phosphates in wastewater at low pH regions (Koh et al., 2020; Leo et al., 2011). However, this only concentrates these phosphates and does not yet recover them; the concentrated stream can still contain impurities that need to be removed and requires further processing. Additionally, the use of membranes makes the technology capital-intensive. In this study, a new approach to recover phosphate more effectively from acidic liquid streams is presented. The idea was inspired by acidic soils literature (pH = 3–5.7) where $FePO_4 \cdot 2H_2O$ strengite-like minerals (strengite and metastrengite) are reported to be naturally formed (Chakravarti and Talibudeen, 1962; Iuliano et al., 2007; Oxmann and Schwendenmann, 2014). Recovering $FePO_4 \cdot 2H_2O$ from acidic waste streams would have advantages over conventional phosphorus recovery products because: 1) no need for chemical dosing to adjust the pH compared to struvite, calcium phosphates, or vivianite; 2) it is insoluble under acidic conditions; 3) it has Fe:P ratio = 1 which means less iron dosing compared to vivianite Fe: P = 1.5; 4) compared to vivianite precipitation, it does not require reducing conditions to form so it can form in the ambient conditions of any WWTP; and 5) the precipitated product will be cleaner and purer, e.g., compared to high pH precipitation products because of high solubility of heavy metals under these low pH conditions (Ain Zainuddin et al., 2019; Marchioretto et al., 2005).

According to $FePO_4 \cdot 2H_2O$ crystallization literature, at room temperature, amorphous Fe (III) phosphates would initially form and then transform into crystalline structures after prolonged aging (Hsu, 1982) . Additionally, $FePO_4 \cdot 2H_2O$ formation at pH 1.6 after 12 h of reaction at 50 and 100 °C was reported to be amorphous and persisted for a substantial time. However, at 200 °C, crystalline strengite and metastrengite formed (Roncal-Herrero et al., 2009). Accordingly, It is expected that $FePO_4 \cdot 2H_2O$ formed under WWTPs ambient conditions will be amorphous, not crystalline, and settle poorly. $FePO_4 \cdot 2H_2O$ recovery from synthetic effluents was reported in earlier studies in which a phosphate recovery percentage of 95 % was achieved, and product settleability was improved by adding carriers in fluidized bed reactors (Priambodo et al., 2017; Xing et al., 2021).

In this study, our approach was to enhance the settleability of $FePO_4 \cdot 2H_2O$ to the level that gravity-based separation techniques are sufficient, without the need for crystallizers or seed material, while maintaining an acceptable recovery via varying operating conditions. First, the optimum initial pH (1.5-5) for recovery was tested. Then, temperature (25–80 °C) was tested as a way to induce partial crystallization and better settleability of the precipitate at higher temperatures. Controlled Fe (III) supply was also tested to prevent high supersaturation, where nucleation dominates over crystal growth, and to improve settleability. Different Fe (III) dosing rates, Fe (II), and different oxidation conditions (pO_2 = 0.2 bar, 1 bar, and 1.5 bar, and different H_2O_2 dosing rates) were tested. The novelty of our research lies in presenting a Fe^{2+} controlled oxidation system via H_2O_2 wherein both high recovery and rapid precipitate settleability are achieved by controlling the supply of Fe (III) through controlled Fe(II) oxidation, without the need to add carriers or further crystallizers, as previously reported in the literature (Priambodo et al., 2017; Xing et al., 2021). The $FePO_4 \cdot 2H_2O$ precipitate was characterized using ICP, SEM, optical microscope, XRD, Raman spectroscopy, and SQUID. Precipitate settleability was also measured using Imhoff sedimentation cones, and volume indexes were calculated in ml/gP.

2. Methodology

2.1. Reagents

$FeNH_4(SO_4)_2.12H_2O$, Fe $(NH_4)_2(SO_4)_2.6H_2O$, and $NH_4H_2PO_4$ salts (Sigma-Aldrich) were used for precipitation experiments adopted from Lundager et al., 2018 protocol. 1M NaOH was prepared with ≈99 % pure NaOH pellets to adjust the initial pH in experiments (VWR chemicals). 0.01 M H_2O_2 was used for Fe (II) oxidation experiments (VWR chemicals). Milli-Q water was used as a solvent to prepare these solutions.

2.2. Preparations

2.2.1. Fe (III) synthetic experiments

0.085 M equimolar solution of $FeNH_4(SO_4)_2$ as a source of Fe (III) and $NH_4H_2PO_4$ as a P source was prepared. Fe (III) solutions were initially adjusted by adding 1M NaOH in pH experiments. The temperature was controlled using shaking incubators in different temperature experiments. Fe (III) dosing to the P solution was carried out in two ways: one-time quick addition and drop-wise (for 3 h) using a glass lab decanter funnel while stirring. The solid precipitation was separated from the liquid fraction by centrifugation at 4000xg for 10 min. The precipitate was then washed three times by adding MilliQ water and separated by centrifugation. Both solid and liquid fractions were analyzed.

2.2.2. Fe (II) synthetic experiments

0.085 M equimolar solution of Fe $(NH_4)_2(SO_4)_2.6H_2O$ as a source of Fe (II) and $NH_4H_2PO_4$ as a P source was prepared. Open-air oxidation ($pO_2 = 0.2$ bar) experiments were left on the lab bench overnight and for 10 days at room temperature. Non-pressurized ($pO_2 = 1$ bar) and pressurized ($pO_2 = 1.5$ bar) pure oxygen experiments were performed in serum-stoppered bottles and left overnight. In H_2O_2 oxidation experiments, H_2O_2 was dosed to Fe (II)P equimolar solution: one-time quick and drop-wise (for 4 mins, 10 mins, 3 h) using a glass lab decanter funnel. The dosage of H_2O_2 was calculated according to Fenton's reaction equation (Truong et al., 2004), with a molar ratio Fe: H_2O_2 = 2:1. Solid and liquid fractions were separated and analyzed.

2.2.3. Real acidic waste from EPS extraction installation in Epe WWTP

Acidic liquid samples from the EPS extraction pilot installation in Epe WWTP were collected as an example of complex wastewater, containing organic and inorganic impurities, to confirm the potential of phosphorus recovery from real acidic streams as $FePO_4{\cdot}2H_2O$. Epe WWTP was the first full-scale domestic wastewater treatment plant in the Netherlands to install the innovative aerobic granular sludge (AGS) treatment technology, operated by the water authority Waterschap Vallei en Veluwe. The EPS extraction process is operated as described in detail by Bahgat et al., 2023. AGS goes through an alkaline reactor in which the pH is within 9-11 and the temperature is 80 °C for 2 h, followed by an acidification reactor in which the pH is within 2.5-3 and an acidic phosphate-rich liquid stream is produced as a by-product. To perform the experiments, the phosphate concentration of the acidic stream from EPS extraction was measured, and the dosage of Fe (III) or Fe (II) and H_2O_2 was determined according to the theoretical molar ratios of Fe:P = 1 and Fe: H_2O_2 = 2.

2.2.4. Settling experiments

Precipitate settleability measurements were conducted by pouring 1L samples into Imhoff sedimentation cones and allowing them to settle. The settled solids volume was recorded at 5, 10, and 30 min, and results were recorded as ml/L. Volumetric indexes were calculated as ml/gP recovered.

2.3. Analysis

2.3.1. Elemental and composition analyses

2.3.1.1. Microwave digestion. With the help of microwave digestion, solids and organics are completely decomposed and dissolved in a strong inorganic acid. Concentrated nitric acid was used to fully digest the samples after they were subjected to high temperature and pressure inside the microwave. The purpose of microwave digestion is to enable a quantitative elemental analysis of solid samples using ICP-OES and IC which require aqueous inorganic samples. Samples were digested in an Ethos Easy from Milestone with an SK-15 High-Pressure Rotor. Around 50 mg of solids were put in a Teflon vessel where 10 mL of ultrapure HNO_3 (64.5-70.5 % from VWR Chemicals) was poured. The digester is set to reach 200 °C in 15 min, run at this temperature for 15 min, and cool down for 1 h.

2.3.1.2. ICP-OES (inductively coupled plasma with optical emission spectrometer). The elemental inorganic composition was measured via Inductively Coupled Plasma (Perkin Elmer, type Optima 5300 DV) with an Optical Emission Spectroscopy as a detector (ICP-OES). The device was equipped with an Autosampler, Perkin Elmer, type ESI-SC-4 DX fast, and the data were processed with the software Perkin Elmer WinLab32. The rinse and standard internal solutions were 2 %HNO_3 and 10 mg/L of Yttrium.

2.3.1.3. C/H/N/O elemental analysis. The solid precipitate from the real acidic samples experiments was analyzed using an Elemental analyzer (Mettler Toledo, America) to check the estimate of the organics co-precipitated.

2.3.1.4. IC (ion chromatography). Liquid samples were pre-treated first by filtering the samples through 0.45 μm followed by 0.22 μm membrane filters before analysis. Anions and cations (free dissolved ions) were measured by Metrohm Compact ion chromatograph Flex 930.

2.3.1.5. LCK 320 iron Hach Lange kits. In this study, Fe (II) and Fe (III) were measured using iron Hach Lange kits which depend on the strong Fe (II)-binding ligand phenanthroline. Three molecules of phenanthroline chelate a single Fe (II) molecule to form an orange-red complex. Any Fe (III) ions in the sample are reduced to Fe (II) in a secondary step by ascorbic acid before the complex is formed again. Phenanthroline is better than ferrozine (another standard Fe (II) colorimetric reagent) at low pH samples. Ferrozine can induce reduction and interfere with the reliable measurement of Fe (II) (Anastácio et al., 2008; Jones et al., 2014)

2.3.1.6. Gas chromatography. The gas composition was analyzed using gas chromatography to ensure that the serum bottles were completely purged by pure oxygen in Fe (II) experiments. A glass syringe (1 mL) was connected to the serum bottles, and a sample was collected and analyzed using Micro GC (CP-4900) using argon as carrier gas. The module was connected to a Thermal Conductivity Detector (TCD) for data acquisition, and the Galaxy Chromatography Data System controls the instrument.

2.3.2. Morphology observations

2.3.2.1. SEM (scanned electron microscopy). The dried precipitate was observed under SEM (Jeol JSM-6480LV) to determine the shape and size of the precipitate. The samples were coated with a 10 nm layer of gold at 15 Pa and 25 mA to make the surface electrically conductive. The following settings were applied: Accelerating Voltage: 6 kV, Working distance: 10 mm. The software used was JEOL SEM Control User Interface.

2.3.2.2. Optical microscope. Liquid samples were analyzed under a light microscope. The sample was placed on the glass slide, and then a cover slide was placed. The sample was observed under 4x, 10x, 20x, and 100x magnifications bright field using the Leica (DMI 6000B) stereo microscope and Olympus (Model BX43F) light microscope. The pictures were captured using the Leica Application Suite (LAS V4.6) and cellSens Standard.

2.3.3. Advanced analytical identification techniques

2.3.3.1. XRD (X-ray diffraction). Room-temperature dried samples were used for XRD analysis. The sample was filled in a 0.7 mm glass capillary and tamped so the solid settled. The capillaries were sealed with a burner and mounted in a sample holder. The device used was a Bruker D8 Advance diffractometer with Cu Ka radiation (Coupled $\theta - 2\theta$ scan 10° - 110°, step size 0.030 ° 2θ, counting time per step 2 s). The data evaluation was performed using Burker software DiffracSuite.EVA vs. 6

2.3.3.2. Raman spectroscopy. Raman Spectroscopy was used to compare $FePO_4$ $2H_2O$ prepared from synthetic solution experiments with strengite and metastrengite minerals from the literature. The processed data of samples was obtained from Raman (LabRam Olympus MPlan N 100x/0.9 Lens). The following settings for Raman Analysis were used: Exposition: 100 s, Spectro: Auto, Accumulation: 1 × 8, Binning: 1, Slit: 100 μm, Hole: 100 μm, Laser: 532.13 nm, Grating: 600, Objective: x100, Detector: Synapse CCD, Detector size: 1024. The spectrum was

processed using Origin-pro by performing baseline correction and smoothing.

2.3.3.3. SQUID (superconducting quantum interference device). Field-dependent magnetization (M-H) curves at a temperature of 300 K were measured in an interference devices (SQUID) MPMS-XL magnetometer equipped with a reciprocating sample option (RSO). The SQUID MPMS provides exceptional sensitivity, as high as 10^5 Am2. The typical sample mass used in this work is about 2~3 mg. The temperature range is between 1.7 and 400 K, and the applied magnetic field is up to 5 T.

2.4. Curve fitting

The nonlinear regression function of Sigma Plot (version 14) was used to fit the phosphorus recovery percentages and volumetric indexes to sigmoidal, 4 parameter function provided in the standard regression library (shown in Eq. (1)), where a is the maximum asymptote, b is the slope, y_0 is the ground asymptote and x_0 is the point of inflection. This function was chosen because the measurement points seemed to behave like a sigmoid function constrained by a pair of horizontal asymptotes (S-shaped curves). The fitting showed an R-squared value of 1 for the P recovery curve and 0.9982 for the volumetric indexes showing the goodness of fit chosen. Details on the fitting are shown in the supplementary material.

$$f = y_0 + \frac{a}{1 + e^{-\left(\frac{x - x_0}{b}\right)}} \quad (1)$$

3. Results

3.1. Evaluation of chemical equilibria

Visual Minteq was utilized for simulating the Fe (III) and phosphate solutions to confirm the potential of $FePO_4{\cdot}2H_2O$ formation under acidic conditions. The inputs included the initial Fe (III) and P concentration in the synthetic solutions, pH, and temperature, as referenced in Section 2.2.1. The calculated saturation indexes indicated $FePO_4{\cdot}2H_2O$ as the only phosphate mineral to form under these conditions. The pKsp used in the calculations is 26.4, as reported by (Nriagu, 1972). As shown in the supplementary material, strengite, goethite, and hematite are supersaturated; however, as discussed later in Section 4.2, the formation of oxide species is almost negligible under the tested acidic conditions. Therefore, only strengite was added to the list of "Possible Solid Phases" The "Equilibrated Mass Distribution" revealed that the fraction of Fe and P precipitate is 99.9 %, indicating that thermodynamically all phosphorus can be recovered as $FePO_4{\cdot}2H_2O$ by the addition of Fe (III).

3.2. pH effect on P recovery%

Fe (III) reacted directly with PO_4^{3-} which led to the instantaneous formation of $FePO_4.2H_2O$ white precipitate in these experiments. The initial pH in Fe (III) experiments was 1.5 upon Fe (III) addition and mixing of the solutions. The effect of pH was studied at room temperature by adjusting the pH from 1.5 to 3, 4, and 5. Total phosphorus (TP) removal from the liquid fraction and TP precipitated are reported in Table 1. pH 3 was the optimum among the tested pH values, achieving a phosphorus recovery rate of approximately 96 %, similar to pH 4 and 5 but with minimal pH adjustment, and surpassing the recovery rate observed at pH 1.5, which stood at 60 %. pH 4 and 5 formed a slightly reddish precipitate, unlike pH 1.5 and 3, indicating a greater formation of hydroxide species at higher pH values. The initial pH dropped by the end of the experiments due to the liberation of H^+ during the precipitation process. Previous literature has also identified pH 3 as optimum for $FePO_4{\cdot}2H_2O$ solubility and purity. The optimal solubility level of $FePO_4{\cdot}2H_2O$ under acidic conditions falls within the range of 2-4, with an optimum value of around 3 (Eastman, 2017; T. Zhang et al., 2017). Additionally, pure $FePO_4{\cdot}2H_2O$ precipitates typically form only below pH 3.5. With increasing pH above 3.5, a mixture of ferric phosphate and hydroxide emerges, with ferric hydroxide precipitates becoming more predominant above pH 4.5 (Morgan and Lahav, 2007a; Takács et al., 2006), further discussion on this is in Section 4.2. Consequently, the initial pH values of our experiments were maintained within the range of 3 and 3.5.

Table 1
Phosphate recovery % in Fe (III) tests (different pH and temperature) and Fe (II) tests (different oxidation conditions). TP% (liquid) is phosphate removal from the liquid fraction measured by IC, and TP% (precipitate) is phosphates recovered as a solid fraction measured by microwave digestion+ ICP, and the molar ratio of Fe:P of the precipitate is calculated. All experiments were performed in triplets, and averages and standard deviations were calculated. The discrepancy between TP% (precipitate) and TP% (liquid) is between 1 % to 6 % and is due to using different instrumental techniques and sample preparation methods to perform the two different measurements.

Synthetic- Fe (III)					
Initial pH	Initial pH	Final pH	TP% (liquid)	TP% (precipitate)	Molar ratio precipitate (Fe:P)
1.5	-	1.3	62 ± 0.0	60 ± 0.3	1.04 ± 0.03
3	-	2.8	98 ± 0.00	94 ± 0.2	1.08 ± 0.01
4	-	3.9	98 ± 0.1	94 ± 0.1	1.07 ± 0.03
5	-	5	98 ± 0.1	94 ± 0.2	1.06 ± 0.00
Temperature					
25°C	1.5	1.3	61 ± 2.0	60 ± 0.3	1.04 ± 0.03
40°C	1.5	1.4	81 ± 0.0	77 ± 0.1	1.03 ± 0.01
60°C	1.5	1.4	87 ± 0.0	84 ± 0.6	1.04 ± 0.00
80°C	1.5	1.3	87 ± 0.00	89 ± 1.0	1.00 ± 0.00
Synthetic- Fe (II) Oxidation to Fe (III)					
Open-air (pO_2 = 0.2 bar)			TP% (liquid)	TP% (precipitate)	Molar ratio (Fe:P)
Overnight	3.5	3.1	9 ± 0.5	5 ± 0.1	0.95 ± 0.01
10 days	3.5	2.7	46 ± 0.3	40 ± 0.2	0.89 ± 0.01
Pure oxygen					
pO_2 = 1 bar-overnight	3.5	2.8	32 ± 1.0	36 ± 0.2	0.90 ± 0.00
pO_2 = 1.5 bar-overnight	3.5	2.6	50 ± 1.0	51 ± 0.1	0.89 ± 0.00
Another oxidant					
H_2O_2	3.5	2.2	99 ± 0.2	98 ± 0.2	1.04 ± 0.02
Stream from the EPS extraction process with a pH of 2.5					
Fe (III)-quick	1.6	1.2	75 ± 0.4	75 ± 0.2	1.02 ± 0.01
Fe (III) -3 h	3	2.6	95 ± 0.3	93 ± 0.2	1.07 ± 0.02
Fe (II) H_2O_2- 3 h	3	2.7	99 ± 0.4	96 ± 0.1	1.04 ± 0.04

3.3. Temperature effect on P recovery%

The effect of temperature was studied at 25, 40, 60, and 80 °C at pH 1.5. The experiment aimed to assess the feasibility of improving settling efficiency by partially crystallizing the precipitate at higher temperatures. This approach was inspired by the observation that crystalline $FePO_4.\ 2H_2O$ formation was reported at elevated temperatures (150–200 °C), as discussed in Section 4.1. In the EPS extraction process, the sludge undergoes heating to 80 °C and then cools down to room temperature before the acidification step. Therefore, the temperature range of room temperature to 80 °C was chosen for testing, as it aligns with the existing process and could potentially be integrated into the acidic by-product stream from the EPS extraction process. Results showed that there was no effect on the crystal size or XRD spectra as discussed in Section 3.6.3. Still, the temperature influenced the phosphorus recovery as shown in Table 1. Higher temperature induced higher phosphorus recovery, increasing temperature from 25 to 40

increased phosphate recovery by 20 %. However, it reached a plateau value as increasing temperature from 60 to 80 °C had negligible effect.

3.4. Fe (II) oxidation effect on P recovery%

In these experiments, Fe (III) was replaced by Fe (II), and it was allowed to oxidize to Fe (III) by O_2 and H_2O_2 and eventually form $FePO_4.2H_2O$. The initial pH in the Fe (II) experiments was 3.5 after the addition of Fe (II) and mixing the solutions. Since Fe (II)-P solutions already fell within the optimal pH range discussed in Section 3.2, there was no need for pH adjustments.

3.4.1. Oxidation via O_2

Phosphate recovery was very low in open-air oxidation systems (pO_2 = 0.2 bar), with approximately 7 % of total phosphorus recovered overnight, as shown in Table 1. When the experiment was extended to 10 days, the recovery increased to approximately 45 %, indicating that more precipitation formed over time, as shown in Fig. 1. These two experiments demonstrated that Fe (II) oxidation under atmospheric conditions is very slow and is the rate-limiting step. One approach to accelerate Fe (II) oxidation under these conditions is by increasing the dissolved oxygen concentration in the system. As the oxygen partial pressure (pO_2) increases, the dissolved oxygen concentration will also increase, following Henry's law. Increasing pO_2 from 0.2 bar to 1 and 1.5 bar with pure oxygen systems was conducted in serum bottles and tested. The recovery increased from approximately 7 % to 34 % and 50 % of the total phosphorus for 1 and 1.5 bar overnight, respectively, as shown in Table 1. Although these results demonstrate that Fe (II) oxidation fastened and recovered phosphorus increased compared to open-air experiments, the low recovery percentage and long duration still pose challenges for WWTPs.

3.4.2. Oxidation via H_2O_2

H_2O_2 is a stronger oxidant than oxygen that can be used to rapidly oxidize Fe (II) to Fe (III). These experiments aimed to increase the speed of the Fe (II) oxidation process by adding H_2O_2. The phosphate recovery in H_2O_2 experiments was higher, approximately around 99 %, close to Fe (III) experiments.

3.5. Fe (III) versus Fe (II) settling

The settling behavior of the precipitate was measured and compared between Fe (II) and Fe (III) experiments. The precipitate formed instantly with the quick addition of Fe (III), and its settleability was poor under all pH and temperature conditions tested, with a volumetric index (VI) equal to 263 ml/gP. However, the controlled addition of Fe (III) for 3 h enhanced the settleability (VI = 40 ml/gP) because of the lower saturation level. Fe (III) formation via Fe (II) oxidation with O_2 and H_2O_2 further enhanced the settleability of the precipitate. Oxygen's slow oxidation resulted in the most settleable precipitate, while H_2O_2 oxidation could influence settling behavior based on how quickly it was added to the Fe (II) system. Comparing H_2O_2 dosage over 3 h, 10 min, 4 min, or one-time addition revealed different settling speeds. These varied oxidation conditions indicate that controlling the Fe (II) oxidation rate is a method to manage the settleability of the precipitate without requiring crystallizers or seed addition. Fe (II) oxidation rates from different experiments were calculated based on Fe (II) consumption over time, as shown in Table 2. Saturation levels could not be measured directly in these experiments as it was impossible to measure Fe^{3+} concentration with the Hach Lange kits because of the instant formation of $FePO_4.2H_2O$ and the low concentrations of Fe^{3+} left in solutions that could not be detected using these kits. Still, an estimation for Fe(III)-(3 h) and Fe(II)-H_2O_2 (3 h) systems could be given based on

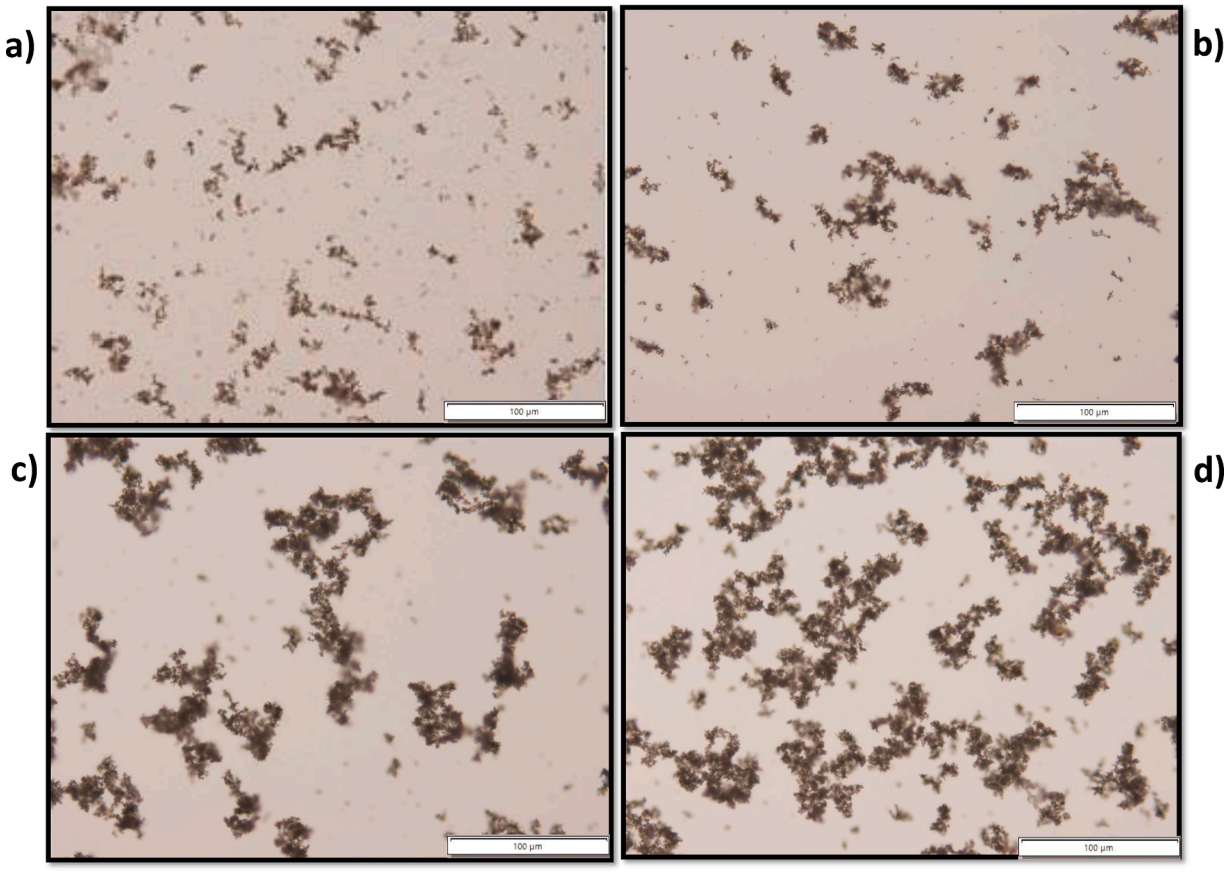

Fig. 1. Fe (III)-P precipitation growth dosing Fe (II) over time under air oxidation conditions pO2 = 0.2 bar (a) 2 days, (b) 4 days, (c) 6 days, (d) 10 days under the optical microscope. Scale = 100µm.

Table 2
Volumetric index of the precipitate formed in different Fe (II) and Fe (III) experiments, calculated by measuring the volume of settled solids after 30 min as ml/g phosphorus and Fe (II) average oxidation rates in different experiments in mol/l/min.

Experimental systems (synthetic)	Volumetric index (ml/gP)	Fe (II) oxidation rate (mol/l/min) *10^{-6}
Fe^{3+}(Quick)	263	-
Fe^{3+}(3 h)	40	-
Fe^{2+}-O_2 0.2 bar (20 h)	2.3	5
Fe^{2+}-O_2 1 bar (20 h)	3	23
Fe^{2+}-O_2 1.5 bar (20 h)	3	35
Fe^{2+}-H_2O_2 (Quick)	250	425000
Fe^{2+}-H_2O_2 (4 mins)	115	21000
Fe^{2+}-H_2O_2 (10 mins)	88	9400
Fe^{2+}-H_2O_2 (3 h)	8	470

one droplet volume (0.05 mL) of F^{3+} solution or H_2O_2 introduced to the P solution and its Fe^{3+} equivalence. The two systems had an initial SI of 2.42, indicating that although the saturation levels were the same, there was a difference in the settling behavior, suggesting that another mechanism besides saturation level is influencing the settleability. The effect of oxidation rate on settling and recovery was fitted to a sigmoidal function as shown in Fig. 2. Combining the phosphate recovery curve (time-dependent) with the settling curve shows an ideal system for recovery that combines both a high recovery percentage and low volumetric index (ml/gP) at Fe (II) oxidation rate of 4.7×10^{-4} mol/l/min. Further characterization of the precipitate from Fe (II)$^{-}H_2O_2$ (3 h) is in Section 3.6.

3.6. FeP precipitate identification

3.6.1. Composition

$FePO_4.2H_2O$ has an equimolar ratio of iron and phosphorus. $FePO_4.2H_2O$ precipitates from all experiments were collected, solubilized, and analyzed by ICP to determine the Fe:P molar ratio as shown in Table 1. In all experiments, the Fe: P molar ratio in the precipitate was around 1; however, for Fe (II)-O_2 oxidation experiments, the ratio was slightly lower (0.89- 0.95), which could indicate another mechanism to remove phosphates besides $FePO_4$ $2H_2O$ formation is taking place (e.g., adsorption).

3.6.2. Morphology

The surface morphology features of the precipitate were demonstrated by SEM (Fig. 3). The precipitate was observed to be agglomerations of small particles in size of 2–3 μm which formed larger clusters in different Fe (III) and Fe (II) experiments. Optical microscope images of the samples showed that the precipitate consists of clusters of small particles (Fig. 4). There was distinction between the precipitates from Fe (II) and Fe (III). In the case of Fe (II), the agglomerations appeared denser and had a stronger dark hue compared to the precipitate from Fe (III). This observation aligns with the superior settling characteristics observed.

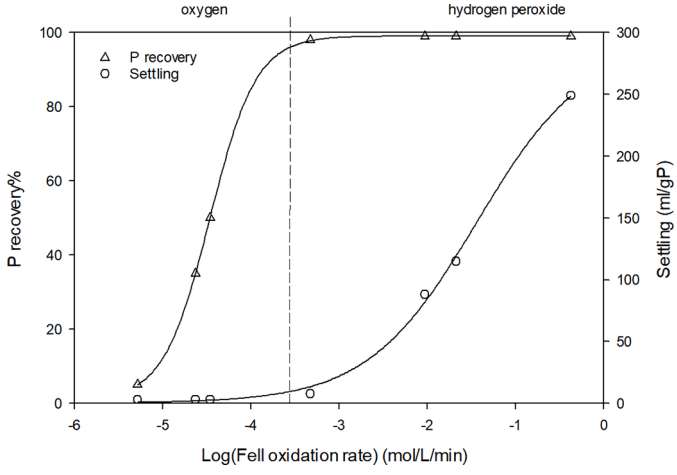

Fig. 2. Log Fe (II) oxidation rate (mol/L/min) versus settling (ml/gP) and P recovery% in both oxygen experiments (slow oxidation) and H_2O_2 experiments (medium to fast oxidation).

3.6.3. Advanced analytical identification

In this section, further characterization of the precipitate from Fe (III) quick addition, Fe (II)-H_2O_2 (3 h), and Fe (II)-O_2 = 0.2 bar (20 h) is provided, as these three points would govern all different experiments tested: no (or rapid) oxidation, Fe (II) ideal rate of oxidation, and Fe (II) slowest oxidation.

Precipitates from Fe (III) quick addition at pH3, Fe (II)- H_2O_2 (3 h), and Fe (II)- pO_2 = 0.2 bar (20 h) had identical XRD spectra. They were all amorphous as no crystalline peaks of $FePO_4.2H_2O$ were visible. Also, the XRD spectra from different temperature experiments showed amorphous precipitate (shown in supplementary material). Fig. 5 shows the measured XRD pattern for the proposed ideal precipitation system of Fe (II)-H_2O_2 (3 h).

Samples from Fe (III) quick addition at pH3, Fe (II)- H_2O_2 (3 h), and Fe (II)- pO_2 = 0.2 bar (20 h) were also analyzed by Raman, (all spectra are shown in the supplementary material), the precipitates showed similar peaks. The Raman spectra of the precipitates were obtained in the region 900–2000 cm^{-1} at 298 K. Peaks at ≈1000 cm^{-1} were ascribed to the stretching vibrations of the $PO4^{3-}$; peaks at ≈ 1600 cm^{-1} were assigned to HOH bending, and other peaks were observed at ≈606, 467, and 248 cm^{-1} (Fig. 5). Precipitates were also analyzed at 298 K by SQUID. The magnetic moment (emu) was measured against the applied magnetic field (Oe). The magnetic susceptibility (emu Oe^{-1} g^{-1}) was calculated based on the slope shown in Eq. (2) and Fig. 5 where M is the material's magnetization, and H is the magnetic field strength. The magnetic susceptibility was 6.7×10^{-5}, 5.4×10^{-5}, and 5.4×10^{-5} emu Oe^{-1} g^{-1} for Fe (III) quick addition at pH3, Fe (II)- H_2O_2 (3 h), and Fe (II)- pO_2 = 0.2 bar (20 h) respectively. The detailed calculations are in the supplementary material.

$$M = x_v H \tag{2}$$

3.7. Proof of principle experiments on acidic by-product stream from EPS extraction process

Acidic samples were collected from the by-product stream from the EPS extraction process from aerobic granular sludge Epe WWTP in the Netherlands (Bahgat et al., 2023); the composition is shown in Table 3. The pH of the waste acidic by-product stream is usually between 2.5-3. The acidic liquid samples collected for these experiments from Epe WWTP had a pH of 2.5. In the first test, the quick addition of Fe (III) to the system without any pH adjustment was tested as it would be the easiest way to recover $FePO_4.2H_2O$ in WWTPs. Similar to synthetic solution, pH dropped to 1.6 upon salt addition (low solubility range) and the recovery was low (75 %). So, to ensure that the initial and final pH is within the optimum range to achieve the highest recovery and purity, it was adjusted to pH 3, and the experiments with a controlled dosage of Fe (III) and Fe (II)-H_2O_2 were performed to evaluate settleability. P recovery values were 95 % and 99 % for Fe (III)-(3 h) and Fe (II)- H_2O_2 (3 h) systems, respectively, with a Fe:P molar ratio of 1 for the dosed Fe. The elemental composition of the precipitates is shown in Table 3, and it shows that organic precipitation also occurred. Additionally, it was observed during the experiments that the precipitate formed was brown, unlike the white precipitate observed in synthetic experiments. Moreover, the acidic liquid after precipitation became much less turbid and less brownish compared to its original state. Based on the percentages of Fe and P in the TS of the precipitate and the theoretical percentage in

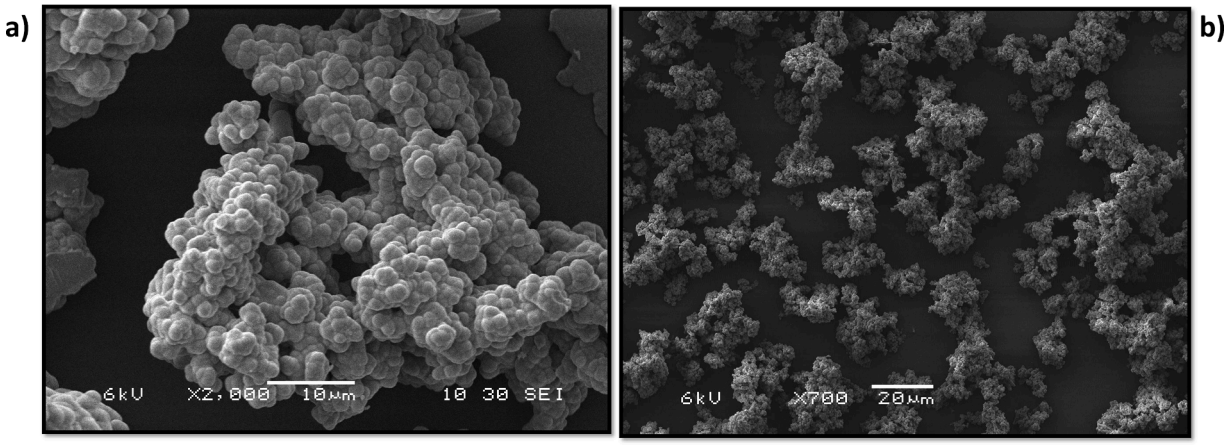

Fig. 3. SEM pictures of the precipitate from Fe (II)- H_2O_2 (3 h) at different magnification levels a) 10 μm and b) 20 μm.

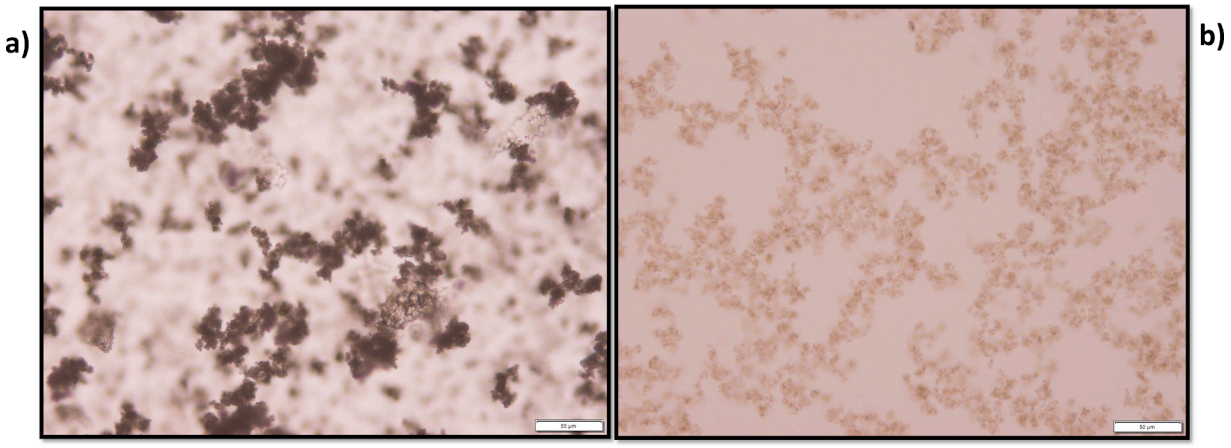

Fig. 4. Microscopic pictures of the wet precipitate from (a) Fe (II) $pO_2 = 0.2$ bar, and (b) Fe^{3+}quick (one-time) addition pH3.

$FePO_4$. $2H_2O$, it is estimated that the purity of the product is around 60–65 %. The difference in precipitate settleability in both Fe (III)- (3 h) and Fe (II)- H_2O_2 (3 h) was not as significant as in the synthetic experiments, as both systems had a volumetric index of 16 ml/gP. The difference between the microscopic pictures in Figs. 6 and 4 showed that the precipitate clusters from the EPS extraction acidic waste stream looked bigger and denser than the synthetic precipitates.

4. Discussion

4.1. $FePO_4.2H_2O$ identification

The formation of tiny particles that tend to agglomerate to form larger clusters or blocks was earlier reported by Lundager Madsen, 2014 and Lundager Madsen and Koch, 2018 when Fe (III) was used to form $FePO_4{\cdot}2H_2O$. They also reported that the precipitate formed under similar ambient conditions is nanocrystalline (XRD amorphous) which fits with our results. These observations align with findings by Hsu, 1982; Reale et al., 2003; Roncal-Herrero et al., 2009, who reported that XRD crystalline $FePO_4{\cdot}2H_2O$ forms only at high temperatures (150–200 °C) and that at ambient temperature range, amorphous phases of $FePO_4{\cdot}2H_2O$ are favored and can persist for a substantial time. The Raman spectrum peaks observed in this study were also compared to crystalline $FePO_4{\cdot}2H_2O$ compounds from the RRUFF database (shown in the supplementary material) and to Frost et al., 2004. The peaks observed at 1016 and 1629 cm^{-1} were similar to those observed in the spectrum for Strengite and metastrengite at around 1000 and 1600 cm^{-1}. Lundager Madsen and Koch, 2018 reported the formation of big orthorhombic crystals when Fe (II) was air oxidized at 35 °C for 15 days. However, this differs from what was observed in this work, as Fe (II) air oxidized at 25 °C for 10 days formed big aggregates of small particles observed by microscopy, while still being amorphous by XRD.

4.2. Fe (II) oxidation in acidic conditions

Fe (II) oxidation experiments showed that Fe (II) oxidation under open atmospheric conditions ($pO_2 = 0.2$ bar) was very limited, and it was accelerated by increasing the oxygen partial pressure ($pO_2 = 1$ and 1.5 bar) or by directly adding H_2O_2 as a replacement of oxygen. The Fe (II) oxidation via O_2 under acidic conditions is the rate-limiting step and how this step is skipped by the addition of H_2O_2 can be explained by the equilibrium chemistry of Fe (II) in aqueous solutions and some models reported in literature. Oxidation of Fe (II) in aqueous solutions is widely reported in the literature due to its presence in wide aquatic contexts such as fresh and marine water environments, acid mine drainage, and industrial water treatment processes. Stumm and Morgan, 1996 presented a kinetic equation for the oxidation of Fe(II) to Fe (III) with $O_{2(aq)}$ as the electron acceptor in which the rate of oxygenation of Fe (II) in solutions of pH $\geq$ 5 is first-order with respect to the concentrations of both Fe (II) and O_2 and second order with respect to the ion OH^-, thus the oxidation reaction rate is strongly pH dependent. At pH 4 or below, the oxidation rate becomes very low and is fundamentally independent of pH. The slow oxidation rate at pH 4 or below can be explained by:

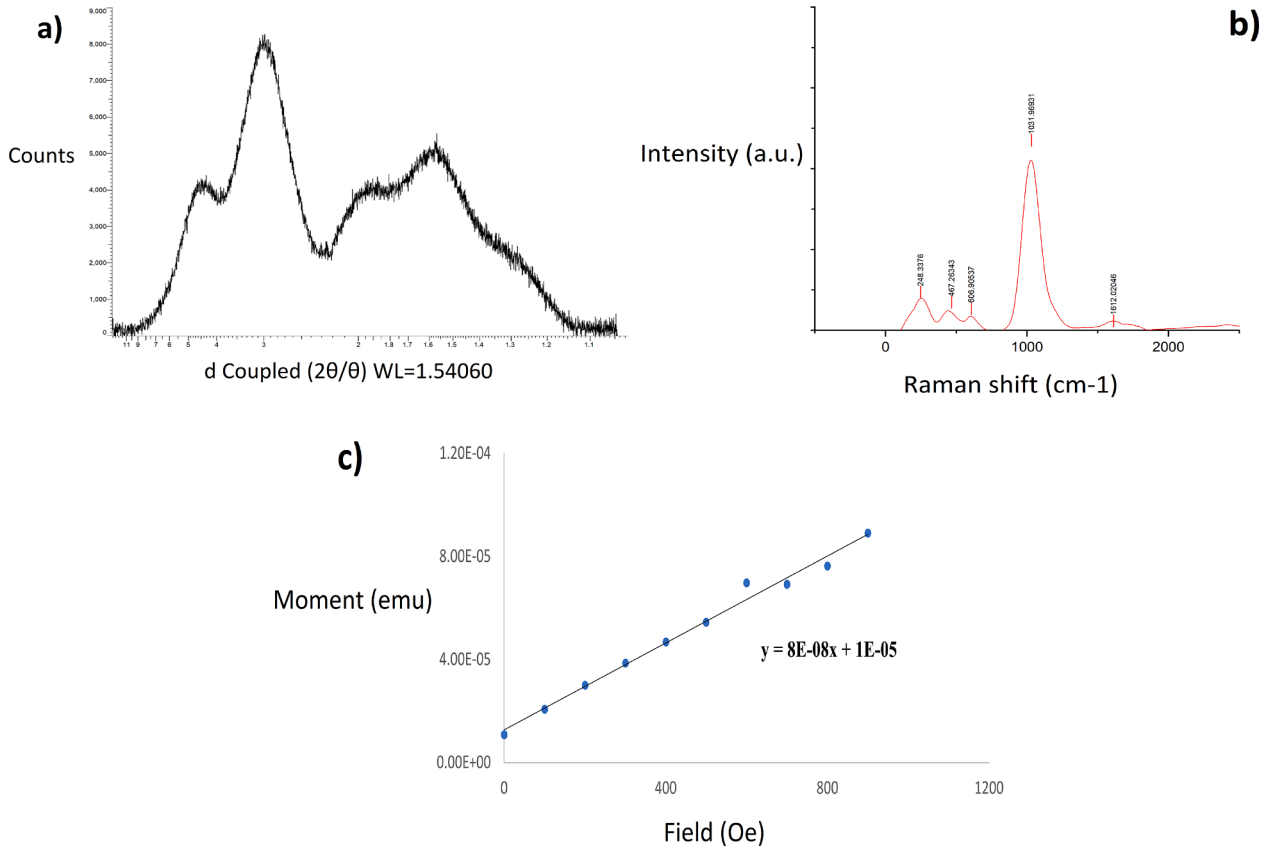

Fig. 5. (a) XRD powder pattern, (b) Raman spectra, and (c) SQUID measurement of the precipitate from Fe (II)- H2O2 (3 h).

Table 3
Elemental composition mg/L of the crude acidic by-product stream from EPS extraction and the TS% of the precipitates from after the addition of Fe.

Elements	EPS-acidic stream (mg/L)	Precipitate (%TS)	
COD	11600	Fe (III)pH3-3 h	Fe (II) H_2O_2-3 h
P	$P\text{-}PO4^{3-}$ = 455, TP = 470	9.9	10.3
Fe	Fe^{2+} = 114, Fe^{3+} = 66, TFe = 185	19.9	20.1
K	4532	0.68	0.9
Al	35	0.07	0.09
Ca	157	0.09	0.13
Mg	78	0.02	0.03
Na	173	0.11	0.12
S	50	1	0.81
C	-	8.5	8.5
H	-	4.0	4.0
N	-	1.3	1.3
O	-	34	37

1) the equilibrium chemistry of Fe (II) in aqueous solutions, Morgan and Lahav, 2007 explained that at pH 4 or below, Fe^{2+} is the most dominant and ferrous hydroxide $FeOH^{+}$and $Fe(OH)_2$ species are almost negligible. Ferrous hydroxide species are the most significant for oxidation, as shown by the reaction constants in Eq. (3).

$$-\frac{d[Fe^{2+}]}{dt} = 6 * 10^{-5}\left[Fe^{2+}\right] + 1.7\ [Fe(OH)^{+}] + 4.3 * 10^{5}\left[Fe(OH)_2^{0}\right] \quad (3)$$

2) as shown in Table 4, thermodynamically, all oxidation steps (1), (2), and (3) are endergonic, but ΔG^0 decreases going from Fe^{2+} to $FeOH^{+}$ and $Fe(OH)_2$ based on the data calculated by Stumm and Morgan, 1996, which explains the faster reaction at higher pH. Also, by combining equation reaction (0) with A, B, C, and D, we can conclude that reaction A is the slowest step and rate-determining as ΔG° for the full reaction is 89.8 kJ/mol, which explains the limited Fe (II) oxidation and P recovery in air oxidation experiments. These ΔG^0 values also show that adding directly H_2O_2 will fasten the Fe (II) oxidation process.

Based on the studies of Lowson, 1982; and Millero (1985), a heuristic model of the oxidation kinetics of Fe (II) to (III) by O_2 was proposed by Morgan and Lahav, 2007 where dFe(II)/dt is the rate of ferrous oxidation in mole per liter per min and rate constants were determined with $pO_2 = 0.2$ bar as shown in Eq. (3). Since Fe^{2+} dominates at conditions below pH 4, so Eq. (3) can be further simplified to Eq. (4). Based on the calculated Fe^{2+} oxidation rate and initial Fe^{2+} concentration in air oxidation experiments ($pO_2 = 0.2$ bar) the oxidation rate constant was calculated to be 6.3×10^{-5} min^{-1}, which is similar to the value suggested by the model.

$$-\frac{d[Fe2+]}{dt} = 6 * 10^{-5}\left[Fe^{2+}\right] \quad (4)$$

4.3. FePO4.2H2O separation methods

4.3.1. Fe (II) systems fast settleability

Improving settleability is an essential parameter in industrial-scale phosphorus precipitation processes. Quick and good settleability will minimize the loss of the precipitate due to washout, enhance phosphorus recovery efficiency, ensure effluent quality, and minimize separation equipment. Different factors can affect settling velocity, such as size, shape, and density of the precipitated particles (Tarragó et al., 2016). As presented in Table 2, using Fe (II) instead of Fe (III) to precipitate phosphate was better for settleability. The XRD spectra confirm that the

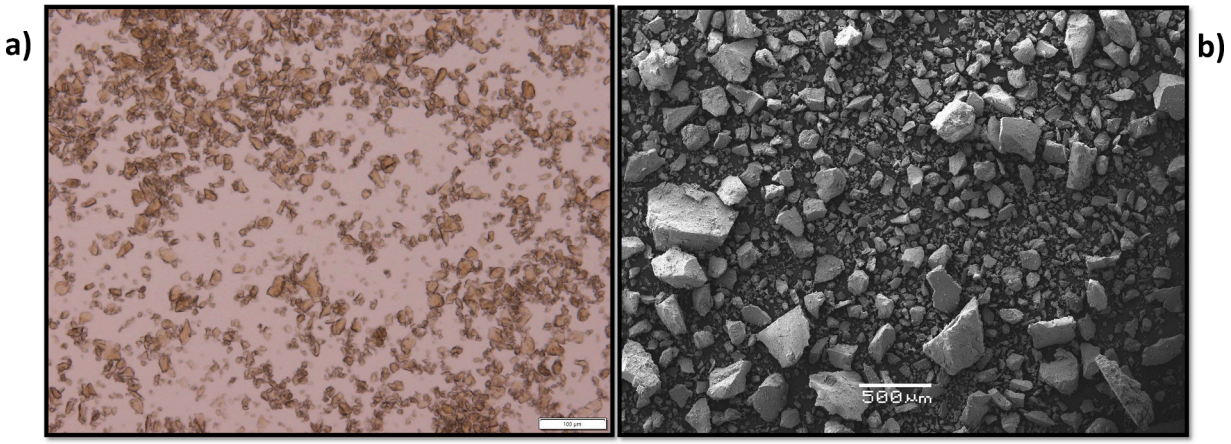

Fig. 6. Iron phosphates precipitate from the acidic by-product stream of the EPS extraction process after dosing Fe (III) - 3 h: a) optical microscope (wet sample) with 100 µm scale, b) SEM (dried sample).

Table 4
ΔG° for the oxidation of Fe (II) and the one-electron steps in the reduction of O_2.

Reaction number	Reaction equation	ΔG^0 (kJ/mol)
0	$Fe^{2+} \rightarrow Fe^{3+} + e^-$	74.2
1	$FeOH^+ \rightarrow FeOH^{2+} + e^-$	48.0
2	$Fe(OH)_2 \rightarrow Fe(OH)_2^+ + e^-$	3
A	$O_{2(aq)} + e^- \rightarrow O_2^-(aq)$	15.5
B	$O_2^-(aq) + e^- + 2\,H^+ \rightarrow H_2O_{2(aq)}$	-165.9
C	$H_2O_{2(aq)} + e^- + H^+ \rightarrow OH_{(aq)} + H_2O$	-95.3
D	$OH_{(aq)} + e^- + H^+ \rightarrow H_2O$	-244.9

precipitates in both Fe (II) and Fe (III) systems are amorphous, so the formation of bigger crystals is not the reason behind the improved settleability. The aggregates formed in both Fe (II)-O_2 or H_2O_2 systems appear bigger and denser, and the color of the particles under the microscope is more pronounced compared to Fe (III), as shown in the microscopic and SEM pictures in Figs. 3 and 4. These denser aggregates in Fe (II) systems can be explained based on differences in surface charge (Kofina and Koutsoukos, 2005; Le Corre et al., 2007) or the effect of low initial supersaturation, which causes the metastable zone to be maintained for a longer time during growth; hence, particle aggregation is improved (Shaddel et al., 2019).

The volumetric index of the $FePO_4\,2H_2O$ (strengite-like precipitates) calculated in the results Section 3.5 was compared to previous indexes reported for magnesium and potassium struvite. Volumetric indexes were reported as 116 ml/gP for the conventional Mg-struvite precipitation approach, and 15 ml/gP for a new approach using microwave-induced decomposition product of struvite pellet to achieve good solid-liquid separation of Mg-struvite by Chen et al. (2020). Wilsenach et al. (2007) also reported VI = 44 ml/gP and 310–500 ml/gP for Mg and K-struvite, respectively. This comparison reflects that the ideal point chosen from our experiments (Fe (II) oxidation rate = 4.7×10^{-4} mol/l/min) indeed exhibits excellent settleability compared to common precipitation practices, as it had a volumetric index of only 8 ml/gP. Although Fe (II) oxidation by O_2 (slow oxidation) can further lower the VI of the precipitate to 2–3 ml/gP, it requires a long retention time to achieve acceptable recoveries, which is problematic in practice.

4.3.2. Magnetic separation

This research showed that excellent settleability of $FePO_4.2H_2O$ can be achieved, and the use of simple settling tanks is possible; however, magnetic separation of the precipitate is also possible. Precipitate characterization showed that $FePO_4\,2H_2O$ precipitates are magnetic both from Fe (II) and Fe (III) systems. Mass susceptibility measurements were 6.7×10^{-5}, 5.4×10^{-5}, and 5.4×10^{-5} emu Oe^{-1} g^{-1} for Fe (III) quick addition, Fe (II)-H_2O_2 (3 h), and Fe (II)- pO_2 = 0.2 bar (20 h), respectively. These measurements were in the same order of magnitude as the calculated values 6.74×10^{-5} emu Oe^{-1} g^{-1} for strengite and 6.37 × 10-5 emu Oe^{-1} g^{-1} for meta-strengite from molar susceptibility data reported by Kim (2009). However, little to no literature on strengite magnetic susceptibility exists. These measurements are significantly higher (x100) than the values reported for vivianite 8×10^{-7} emu Oe^{-1} g^{-1} (Minyuk et al., 2013). ViviMag is an upscaling project for the magnetic separation of vivianite from digested sewage sludge (Wijdeveld et al., 2022). Since $FePO_4.\,2H_2O$ precipitates have higher magnetic susceptibility, this could potentially allow for higher recovery/separation compared to vivianite with the same magnetic strength. This advanced separation technique can be useful for toxic or high organic load waste streams where co-settling can be problematic.

4.4. Proof of principle experiments on acidic by-product stream from EPS extraction process

Proof-of-principle experiments on the acidic samples from the EPS extraction process from AGS WWTPs were conducted to confirm the potential of integrating this technology to recover phosphorus from EPS installations. Experiments showed that the theoretical iron dosage to maintain the Fe: P molar ratio at 1 and the theoretical H_2O_2 dosage to maintain Fe: H_2O_2 at 2 were sufficient to achieve a phosphate recovery of over 95 %. This was surprising, as it was expected that a higher Fe or H_2O_2 dosage would be required due to the presence of organics in these samples (COD = 11600 mg/L). Complexation of Fe by organic matter presence was reported in the literature to alter iron speciation, redox reactivity by manipulating the energetics of the Fe (III)/Fe (II) redox couple, and possible electron transfer reactions (Wang et al., 2013). The Fenton reaction is widely reported to oxidize organic micropollutants under acidic conditions (Ijpelaar et al., 2002). Organics precipitated with $FePO_4.\,2H_2O$ as shown in the precipitate elemental analysis in Table 3 which was also observed during settling experiments as large brown filaments were observed to settle in both Fe (III) and Fe (II) systems. Both systems exhibited a good volumetric index for the precipitate equal to 16 ml/gP, as the presence of organics significantly improved the settleability of the Fe (III) system. The exact mechanistic explanation of why organics enhance aggregation and settling is not clear yet in this study, but the presence of a high organic load could have altered the charge of the $FePO_4.2H_2O$ particles, leading to their rapid settleability in Fe (III) systems, making it comparable to the Fe (II)-H_2O_2 system (Angelico et al., 2014; Dalas et al., 1990). It is shown that Fe (III) can be added to the current EPS extraction installations to achieve high phosphate recovery and good settleability instead of the Fe (II)-H_2O_2 system. However, to obtain a pure product, it may be necessary,

depending on the intended application, to remove the organics priorly with ultrafiltration to prevent undesired precipitation and utilize the Fe (II)-H_2O_2 system instead.

5. Outlook

The recovery of phosphorus as $FePO_4{\cdot}2H_2O$ (strengite-like compounds) from acidic waste liquid streams represents a novel research avenue, yet numerous research gaps remain to be explored. The primary research gap pertains to the fundamental understanding of $FePO_4{\cdot}2H_2O$ formation in the presence of Fe (II)-H_2O_2, aiming to determine whether the regulation of supersaturation, charge, or both accounts for the denser agglomeration and rapid settleability observed in these systems. It is also proposed to perform particle size measurements for the precipitate to confirm that the formation of larger agglomerations in Fe (II)-H_2O_2 systems contributes to improved settleability. The second research gap involves the process optimization of real waste streams and the potential challenges associated with upscaling. It would be intriguing to evaluate other acidic municipal and industrial streams and to assess the functionality of the Fe (II)-H_2O_2 system. Although our experiments were not conducted at different initial concentrations, the outcomes based on the Fe (II) oxidation rate versus recovery and settleability curve are still anticipated. A higher concentration of phosphorus would necessitate a slower addition of Fe (II) to the system to achieve the optimum Fe (II) oxidation rate. For lower concentrations, Fe (II) addition would be quicker, resulting in a faster process, which is advantageous. However, dedicated experiments to investigate the formation mechanism should be conducted in future research to also evaluate if the surface charge (e.g., measuring zeta potential) plays a role in settleability and if changing the concentrations would influence the surface charge, as it alters the saturation levels.

To facilitate the potential scale-up of the technology, it is also recommended to conduct a detailed economic analysis of the Fe (II)-H_2O_2 method of phosphorus recovery, comparing it with other conventional phosphorus recovery processes such as struvite or vivianite recovery. At this stage, an estimation of economic comparison based on OPEX (operating expenses, e.g., Fe salt usage, addition of chemicals such as NaOH or KOH, and H_2O_2) has been performed. The analysis indicates that the recovery of $FePO_4{\cdot}2H_2O$ via the Fe (II)- H_2O_2 method will be at least 2 times more cost-effective than vivianite recovery from EPS extraction acidic by-product stream. Detailed calculations are provided in the supplementary material. Although the CAPEX remains unknown at this stage, it is anticipated that it will be lower for $FePO_4{\cdot}2H_2O$ recovery due to the novel method developed in this study, which enables the recovery of gravity-settleable precipitates without the need for engineered crystallizers, as required by vivianite recovery. The third research gap involves evaluating and testing the potential applications of such recovery products in fertilization or the manufacturing process of electrode materials, catalysts, precursors of $LiFePO_4$, or as an adsorbent for lead pollutants (Li et al., 2020; Reale et al., 2003; Y. Wang et al., 2018; Zhou et al., 2017). This would require double-checking the purity of $FePO_4.2H_2O$ recovered from different acidic streams, and how it is comparable to calcium phosphates, struvite, or vivianite.

6. Conclusion

Recovery of $FePO_4.2H_2O$ from acidic streams appears promising due to its simplicity and high efficiency, while also reducing the need for pH adjustment and excessive usage of ferric salts. However, an integrated optimization of recovery efficiency and product properties (aggregation and settling) is necessary to achieve feasible recovery from low pH and phosphate-rich streams. This research presents a novel strategy to integrate Fe (II) and H_2O_2 controlled dosing systems as the best approach to achieve high P% recovery (> 95 %) and form a quick-settling precipitate with a volumetric index equal to only 8 ml/gP. The Fe (II) oxidation rate is the design parameter to enhance the settling process without adding a carrier material or further crystallizer reactors. Extremely low Fe (II) oxidation rates will result in a quick-settling precipitate but a low recovery percentage over long durations, while rapid oxidation rates will result in a high recovery percentage over short durations but poor settleability. Accordingly, the oxidation rate value of 4.7×10^{-4} mol/l/min was the optimum point for achieving both high recovery and settling. Experiments on the acidic by-product stream from EPS extraction installations confirmed high phosphate recovery (> 95 %) while dosing the theoretical amounts of Fe and H_2O_2. Additionally, the organics present in that stream enhanced aggregation and settling. The mechanism is not yet fully understood, requiring further experiments in future research. $FePO_4.2H_2O$ compounds have potential applications in fertilization, lithium batteries, and electrode materials production.

CRediT authorship contribution statement

Nouran T. Bahgat: Writing – review & editing, Writing – original draft, Visualization, Methodology, Investigation, Formal analysis, Data curation, Conceptualization. **Aamash Siddiqui:** Methodology, Investigation, Formal analysis, Data curation. **Philipp Wilfert:** Writing – review & editing, Supervision, Methodology, Formal analysis, Conceptualization. **Leon Korving:** Writing – review & editing, Supervision, Investigation, Funding acquisition, Conceptualization. **Mark C. M. van Loosdrecht:** Writing – review & editing, Supervision, Funding acquisition, Conceptualization.

Declaration of competing interest

The authors declare that they have no known competing financial interests or personal relationships that could have appeared to influence the work reported in this paper.

Data availability

Data will be made available on request.

Acknowledgments

This work has received funding from the European Union's Horizon 2020 research and innovation program under grant agreement No 869474' 'The opinions expressed in this document reflect only the author's view and reflect in no way the European Commission's opinions. The European Commission is not responsible for any use that may be made of the information it contains. A special thanks go to Alexander Groen, from Waterschap Vallei en Veluwe, Wim Borgonje, Leo Sorin, and Thomas Prot from Wetsus. Thanks to all Wetsus theme members and Water Mining EU partners within WP 4 for fruitful discussions.

Supplementary materials

Supplementary material associated with this article can be found, in the online version, at doi:10.1016/j.watres.2024.121905.

References

Ain Zainuddin, N., Azwan Raja Mamat, T., Imam Maarof, H., Wahidah Puasa, S., Rohana Mohd Yatim, S., 2019. Removal of nickel, zinc and copper from plating process industrial raw effluent via hydroxide precipitation versus sulphide precipitation. IOP Conf. Ser.: Mater. Sci. Eng. 551 (1) https://doi.org/10.1088/1757-899X/551/1/012122.

Anastácio, A.S., Harris, B., Yoo, H.I., Fabris, J.D., Stucki, J.W., 2008. Limitations of the ferrozine method for quantitative assay of mineral systems for ferrous and total iron. Geochim. Cosmochim. Acta 72 (20). https://doi.org/10.1016/j.gca.2008.07.009.

Angelico, R., Ceglie, A., He, J.Z., Liu, Y.R., Palumbo, G., Colombo, C., 2014. Particle size, charge and colloidal stability of humic acids coprecipitated with ferrihydrite. Chemosphere 99. https://doi.org/10.1016/j.chemosphere.2013.10.092.

Ashley, K., Cordell, D., Mavinic, D., 2011. A brief history of phosphorus: from the philosopher's stone to nutrient recovery and reuse. Chemosphere 84 (6). https://doi.org/10.1016/j.chemosphere.2011.03.001.

Bahgat, N.T., Wilfert, P., Korving, L., van Loosdrecht, M., 2023. Integrated resource recovery from aerobic granular sludge plants. Water. Res. 234 https://doi.org/10.1016/j.watres.2023.119819.

Carvalho, F., Prazeres, A. R., & Rivas, J. (2013). Cheese whey wastewater: characterization and treatment. In *Science of the Total Environment* (Vols. 445–446). https://doi.org/10.1016/j.scitotenv.2012.12.038.

CHAKRAVARTI, S.N., TALIBUDEEN, O., 1962. Phosphate equilibria in acid soils. J. Soil Sci. 13 (2) https://doi.org/10.1111/j.1365-2389.1962.tb00701.x.

Chen, S., Yang, Y., Zheng, M., Cheng, X., Xu, K., Dou, X., 2020. Thermal decomposition of struvite pellet by microwave radiation and recycling of its product to remove ammonium and phosphate from urine. Environ. Res. 188 https://doi.org/10.1016/j.envres.2020.109774.

Childers, D.L., Corman, J., Edwards, M., Elser, J.J., 2011. Sustainability challenges of phosphorus and food: solutions from closing the human phosphorus cycle. Bioscience 61 (2). https://doi.org/10.1525/bio.2011.61.2.6.

Cichy, B., Kużdżał, E., Krztoń, H., 2019. Phosphorus recovery from acidic wastewater by hydroxyapatite precipitation. J. Environ. Manage 232. https://doi.org/10.1016/j.jenvman.2018.11.072.

Dalas, E., Koutsoukos, P., Karaiskakis, G., 1990. The effect of carrier solution on the particle size distribution of inorganic colloids measured by steric field-flow fractionation. Colloid Polym. Sci. 268 (2) https://doi.org/10.1007/BF01513194.

Danalewich, J.R., Papagiannis, T.G., Belyea, R.L., Tumbleson, M.E., Raskin, L., 1998. Characterization of dairy waste streams, current treatment practices, and potential for biological nutrient removal. Water. Res. 32 (12) https://doi.org/10.1016/S0043-1354(98)00160-2.

Desmidt, E., Ghyselbrecht, K., Zhang, Y., Pinoy, L., Van Der Bruggen, B., Verstraete, W., Rabaey, K., Meesschaert, B., 2015. Global phosphorus scarcity and full-scale P-recovery techniques: a review. Crit. Rev. Environ. Sci. Technol. 45 (4) https://doi.org/10.1080/10643389.2013.866531.

Doyle, J.D., Parsons, S.A., 2002. Struvite formation, control and recovery. The authors declare that they have no known competing financial interests or personal relationships that could have appeared to influence the work reported in this paper. Water Res. 36 (16) https://doi.org/10.1016/S0043-1354(02)00126-4. VolIssue.

Eastman, K. (2017). *Digital commons @ Montana tech supergene mineralization of the continental PIT, BUTTE, Silver Bow County, Montana.* https://digitalcommons.mtech.edu/grad_rschhttp://digitalcommons.mtech.edu/grad_rsch/125.

Eicher, N. (2018). The LeachPhos process at the waste-to-energy plant Bern (Switzerland). In *Phosphorus: Polluter and Resource of the Future – Removal and Recovery from Wastewater*. https://doi.org/10.2166/9781780408361_411.

ESPP webinar. (2020). *Summary of joint European Commission-ESPP webinar on P4 (phosphorus) Critical Raw Material.* www.phosphorusplatform.eu.

Eynard, U., Wittmer, D., Latunussa, C., & Di Milano, P. (2020). *Study on the EU's list of critical raw materials (2020) non-critical raw materials factsheets safewater view project design for sustainability Fiji view project*. https://doi.org/10.2873/587825.

Frossard, E., Bauer, J.P., Lothe, F., 1997. Evidence of vivianite in FeSO4 - flocculated sludges. Water. Res. 31 (10) https://doi.org/10.1016/S0043-1354(97)00101-2.

Frost, R.L., Weier, M.L., Erickson, K.L., Carmody, O., Mills, S.J., 2004. Raman spectroscopy of phosphates of the variscite mineral group. J. Raman Spectrosc. 35 (12), 1047–1055. https://doi.org/10.1002/jrs.1251.

Hsu, P.H., 1982. Crystallization of Iron(III) phosphate at room temperature. Soil Sci. Soc. Am. J. 46 (5) https://doi.org/10.2136/sssaj1982.03615995004600050009x.

Ijpelaar, G.F., Groenendijk, M., Kruithof, J.C., Schippers, J.C., 2002. Fenton process for the combined removal of iron and organic micropollutants in groundwater treatment. Water Sci. Technol.: Water Supply 2 (2). https://doi.org/10.2166/ws.2002.0068.

Iuliano, M., Ciavatta, L., De Tommaso, G., 2007. On the solubility constant of strengite. Soil Sci. Soc. Am. J. 71 (4) https://doi.org/10.2136/sssaj2006.0109.

Iwama, T., Du, C.M., Koizumi, S., Gao, X., Ueda, S., Kitamura, S.Y., 2020. Extraction of phosphorus and recovery of phosphate from steelmaking slag by selective leaching. ISIJ Int. 60 (2) https://doi.org/10.2355/isijinternational.ISIJINT-2019-298.

Jones, A.M., Griffin, P.J., Collins, R.N., Waite, T.D., 2014. Ferrous iron oxidation under acidic conditions - The effect of ferric oxide surfaces. Geochim. Cosmochim. Acta 145. https://doi.org/10.1016/j.gca.2014.09.020.

Kim, J. (2009). *Investigation of surface adsorption of Li + and phosphate on iron oxyhydroxides via solid-state NMR spectroscopy*. https://dspace.sunyconnect.suny.edu/bitstream/handle/1951/52354/000000842.sbu.pdf?sequence=1.

Kofina, A.N., Koutsoukos, P.G., 2005. Spontaneous precipitation of struvite from synthetic wastewater solutions. Cryst. Growth Des. 5 (2) https://doi.org/10.1021/cg049803e.

Koh, K.Y., Zhang, S., Chen, J.P., 2020. Improvement of ultrafiltration for treatment of phosphorus-containing water by a Lanthanum-Modified aminated polyacrylonitrile membrane. ACS Omega 5 (13). https://doi.org/10.1021/acsomega.9b03573.

Kratz, S., Schick, J., Schnug, E., 2016. Trace elements in rock phosphates and P containing mineral and organo-mineral fertilizers sold in Germany. Sci. Total Environ. 542 https://doi.org/10.1016/j.scitotenv.2015.08.046.

Le Corre, K.S., Valsami-Jones, E., Hobbs, P., Jefferson, B., Parsons, S.A., 2007. Struvite crystallisation and recovery using a stainless steel structure as a seed material. Water. Res. 41 (11) https://doi.org/10.1016/j.watres.2007.03.002.

Lei, Y., Zhan, Z., Saakes, M., van der Weijden, R.D., Buisman, C.J.N., 2022. Electrochemical recovery of phosphorus from acidic cheese wastewater: feasibility, quality of products, and comparison with chemical precipitation. ACS ES T Water 1 (4). https://doi.org/10.1021/acsestwater.0c00263.

Leo, C.P., Chai, W.K., Mohammad, A.W., Qi, Y., Hoedley, A.F.A., Chai, S.P., 2011. Phosphorus removal using nanofiltration membranes. Water Sci. Technol. 64 (1) https://doi.org/10.2166/wst.2011.598.

Li, R., Li, Q., Sun, X., Li, J., Shen, J., Han, W., Wang, L., 2020. Removal of lead complexes by ferrous phosphate and iron phosphate: unexpected favorable role of ferrous ions. J. Hazard. Mater. 392 https://doi.org/10.1016/j.jhazmat.2020.122509.

Lowson, R.T., 1982. Aqueous oxidation of pyrite by molecular oxygen. Chem. Rev. 82 (5) https://doi.org/10.1021/cr00051a001.

Lundager Madsen, H.E., 2014. Redox process catalysed by growing crystal - Strengite, FePO4,2H2O, crystallizing from solution with iron(II) and hydroxylamine. J. Cryst. Growth 401. https://doi.org/10.1016/j.jcrysgro.2013.11.025.

Lundager Madsen, H.E., Koch, C.B., 2018. Kinetics of solution crystal growth of strengite, FePO4,2H2O. J. Cryst. Growth 482. https://doi.org/10.1016/j.jcrysgro.2017.10.014.

Luyckx, L., Sousa Correia, D.S., Van Caneghem, J., 2021. Linking phosphorus extraction from different types of biomass incineration ash to ash mineralogy, ash composition and chemical characteristics of various types of extraction liquids. Waste BioMass Valoriz. 12 (9) https://doi.org/10.1007/s12649-021-01368-3.

Marchioretto, M.M., Bruning, H., Rulkens, W., 2005. Heavy metals precipitation in sewage sludge. Sep. Sci. Technol. (16), 40. https://doi.org/10.1080/01496390500423748.

(Lek) Martin, N., Ya, V., Leewiboonsilp, N., Choo, K.H., Noophan, P., Li, C.W., 2020. Electrochemical crystallization for phosphate recovery from an electronic industry wastewater effluent using sacrificial iron anodes. J. Clean. Prod. 276. https://doi.org/10.1016/j.jclepro.2020.124234.

Metcalf, W., & Eddy, C. (2014). Wastewater Engineering: Treatment and Resource Recovery, Fifth Edition. In *Wastewater Engineering: Treatment and Resource Recovery, Fifth Edition*.

Meyer, C., Preyl, V., Steinmetz, H., Maier, W., Mohn, R.E., Schönberger, H., 2018. The stuttgart process (Germany). Phosphorus Recovery and Recycling. https://doi.org/10.1007/978-981-10-8031-9_19.

Millero, F.J., 1985. The effect of ionic interactions on the oxidation of metals in natural waters. Geochim. Cosmochim. Acta 49 (2). https://doi.org/10.1016/0016-7037(85)90046-8.

Minyuk, P.S., Subbotnikova, T.V., Brown, L.L., Murdock, K.J., 2013. High-temperature thermomagnetic properties of vivianite nodules, Lake El'gygytgyn, Northeast Russia. Clim. Past 9 (1). https://doi.org/10.5194/cp-9-433-2013.

Monat, L., Zhang, W., Jarošíková, A., Haung, H., Bernstein, R., Nir, O., 2022. Circular process for phosphoric acid plant wastewater facilitated by selective electrodialysis. ACS Sustain. Chem. Eng. 10 (35) https://doi.org/10.1021/acssuschemeng.2c03132.

Morgan, B., Lahav, O., 2007a. The effect of pH on the kinetics of spontaneous Fe(II) oxidation by O2 in aqueous solution - basic principles and a simple heuristic description. Chemosphere 68 (11). https://doi.org/10.1016/j.chemosphere.2007.02.015.

Morgan, B., Lahav, O., 2007b. The effect of pH on the kinetics of spontaneous Fe(II) oxidation by O2 in aqueous solution - basic principles and a simple heuristic description. Chemosphere 68 (11). https://doi.org/10.1016/j.chemosphere.2007.02.015.

Nawghare, P., Rao, N.N., Bejankiwar, R., Szyprkowicz, L., Kaul, S.N., 2001. Treatment of phosphoric acid plant wastewater using Fenton's reagent and coagulants. J. Environ. Sci. Health - Part A Toxic/Hazard. Substanc. Environ. Eng. 36 (10) https://doi.org/10.1081/ESE-100107444.

Nriagu, J.O., 1972. Solubility equilibrium constant of strengite. Am. J. Sci. 272 (5) https://doi.org/10.2475/ajs.272.5.476.

Oxmann, J.F., Schwendenmann, L., 2014. Quantification of octacalcium phosphate, authigenic apatite and detrital apatite in coastal sediments using differential dissolution and standard addition. Ocean Sci. 10 (3) https://doi.org/10.5194/os-10-571-2014.

Priambodo, R., Shih, Y.J., Huang, Y.H., 2017a. Phosphorus recovery as ferrous phosphate (vivianite) from wastewater produced in manufacture of thin film transistor-liquid crystal displays (TFT-LCD) by a fluidized bed crystallizer (FBC). RSC Adv. 7 (65) https://doi.org/10.1039/c7ra06308c.

Priambodo, R., Shih, Y.J., Huang, Y.H., 2017b. Phosphorus recovery as ferrous phosphate (vivianite) from wastewater produced in manufacture of thin film transistor-liquid crystal displays (TFT-LCD) by a fluidized bed crystallizer (FBC). RSC Adv. 7 (65) https://doi.org/10.1039/c7ra06308c.

Reale, P., Scrosati, B., Delacourt, C., Wurm, C., Morcrette, M., Masquelier, C., 2003a. Synthesis and thermal behavior of crystalline hydrated iron(III) phosphates of interest as positive electrodes in Li batteries. Chem. Mater. 15 (26) https://doi.org/10.1021/cm031107z.

Reale, P., Scrosati, B., Delacourt, C., Wurm, C., Morcrette, M., Masquelier, C., 2003b. Synthesis and thermal behavior of crystalline hydrated iron(III) phosphates of interest as positive electrodes in Li batteries. Chem. Mater. 15 (26) https://doi.org/10.1021/cm031107z.

Ridder, M. de. (2012). *Risks and opportunities in the global phosphate rock market : robust strategies in times of uncertainty*. The Hague Centre for Strategic Studies.

Roncal-Herrero, T., Rodríguez-Blanco, J.D., Benning, L.G., Oelkers, E.H., 2009. Precipitation of iron and aluminum phosphates directly from aqueous solution as a function of temperature from 50 to 200°C. Cryst. Growth Des. 9 (12), 5197–5205. https://doi.org/10.1021/cg900654m.

Shaddel, S., Ucar, S., Andreassen, J.P., Sterhus, S.W., 2019. Engineering of struvite crystals by regulating supersaturation - Correlation with phosphorus recovery, crystal morphology and process efficiency. J. Environ. Chem. Eng. 7 (1) https://doi.org/10.1016/j.jece.2019.102918.

Slavov, A.K., 2017. General characteristics and treatment possibilities of dairy wastewater -a review. Food Technol. Biotechnol. 55 (1) https://doi.org/10.17113/ft.b.55.01.17.4520.

Smit, A.L., Bindraban, P.S., Shroeder, J.J., Conijin, J.G., G, V.D.M.H, 2009. Phosphorus in agriculture: global resources, trends and developments. Wageningen, Plant Res. Int. BV 282 (January 2009).

Stumm, Morgan, 1996. Aquatic chemistry: chemical equilibria and rates in natural waters. Choice Rev. Online 33 (11). https://doi.org/10.5860/choice.33-6312.

Takács, I., Murthy, S., Smith, S., McGrath, M., 2006. Chemical phosphorus removal to extremely low levels: experience of two plants in the Washington, DC area. Water Sci. Technol. 53 (12) https://doi.org/10.2166/wst.2006.402.

Tarragó, E., Puig, S., Ruscalleda, M., Balaguer, M.D., Colprim, J., 2016. Controlling struvite particles' size using the up-flow velocity. Chem. Eng. J. 302 https://doi.org/10.1016/j.cej.2016.06.036.

Thant Zin, M. M., & Kim, D. J. (2019). Struvite production from food processing wastewater and incinerated sewage sludge ash as an alternative N and P source: optimization of multiple resources recovery by response surface methodology. *Process Safety and Environmental Protection*, 126. https://doi.org/10.1016/j.psep.2019.04.018.

Truong, G.Le, De Laat, J., Legube, B, 2004. Effects of chloride and sulfate on the rate of oxidation of ferrous ion by H2O2. Water. Res. 38 (9) https://doi.org/10.1016/j.watres.2004.01.033.

van Dijk, K.C., Lesschen, J.P., Oenema, O., 2016. Phosphorus flows and balances of the European Union Member States. Sci. Total Environ. 542 https://doi.org/10.1016/j.scitotenv.2015.08.048.

Wang, Y., Feng, Z., Laul, D., Zhu, W., Provencher, M., Trudeau, M.L., Guerfi, A., Zaghib, K., 2018. Ultra-low cost and highly stable hydrated FePO4 anodes for aqueous sodium-ion battery. J. Power. Sources. 374, 211–216. https://doi.org/10.1016/j.jpowsour.2017.10.088.

Wang, Z., Bush, R.T., Liu, J., 2013. Arsenic(III) and iron(II) co-oxidation by oxygen and hydrogen peroxide: divergent reactions in the presence of organic ligands. Chemosphere 93 (9). https://doi.org/10.1016/j.chemosphere.2013.06.076.

Wijdeveld, W.K., Prot, T., Sudintas, G., Kuntke, P., Korving, L., van Loosdrecht, M.C.M., 2022. Pilot-scale magnetic recovery of vivianite from digested sewage sludge. Water. Res. 212 https://doi.org/10.1016/j.watres.2022.118131.

Wilfert, P., Mandalidis, A., Dugulan, A.I., Goubitz, K., Korving, L., Temmink, H., Witkamp, G.J., Van Loosdrecht, M.C.M., 2016. Vivianite as an important iron phosphate precipitate in sewage treatment plants. Water. Res. 104 https://doi.org/10.1016/j.watres.2016.08.032.

Wilsenach, J.A., Schuurbiers, C.A.H., van Loosdrecht, M.C.M., 2007. Phosphate and potassium recovery from source separated urine through struvite precipitation. Water. Res. 41 (2) https://doi.org/10.1016/j.watres.2006.10.014.

Xing, C., Shi, J., Cui, F., Shen, J., Li, H., 2021. Fe2+/H2O2-strengite method with the enhanced settlement for phosphorus removal and recovery from pharmaceutical effluents. Chemosphere 277. https://doi.org/10.1016/j.chemosphere.2021.130343.

Zhang, J.C., Wu, C.J., Yu, D.M., 2019. Effect of phosphoric acid in the pre-hydrolysis process of dissolving pulp production from Bamboo-willow. BioResources 14 (2). https://doi.org/10.15376/biores.14.2.3117-3131.

Zhang, T., Lu, Y., Luo, G., 2017. Effects of temperature and phosphoric acid addition on the solubility of iron phosphate dihydrate in aqueous solutions. Chin. J. Chem. Eng. 25 (2) https://doi.org/10.1016/j.cjche.2016.06.009.

Zhou, D., Qiu, X., Liang, F., Cao, S., Yao, Y., Huang, X., Ma, W., Yang, B., Dai, Y., 2017. Comparison of the effects of FePO4 and FePO4·2H2O as precursors on the electrochemical performances of LiFePO4/C. Ceram. Int. 43 (16), 13254–13263. https://doi.org/10.1016/j.ceramint.2017.07.023.